J|A|C|S ARTICLES

Published on Web 10/07/2009

Virtual High Throughput Screening Confirmed Experimentally: Porous Coordination Polymer Hydration

John J. Low,* Annabelle I. Benin, Paulina Jakubczak, Jennifer F. Abrahamian, Syed A. Faheem, and Richard R. Willis*

UOP Research Center, UOP LLC, a Honeywell Company, 50 East Algonquin Road, Des Plaines, Illinois 60017

Received July 28, 2009; E-mail: richard.willis@uop.com

Abstract: Hydrothermal stability is a pertinent issue to address for many industrial applications where percent levels of water can be present at temperatures ranging from subambient to several hundred degrees. Our objective is to understand relative stabilities of MOF materials through experimental testing combined with molecular modeling. This will enable the ultimate design of materials with improved hydrothermal stability, while maintaining the properties of interest. The tools that we have employed for these studies include quantum mechanical calculations based upon cluster models and combinatorial steaming methods whereby a steam stability map was formulated according to the relative stability of different materials. The experimental steaming method allows for high throughput screening of materials stability over a broad range of steam levels as well as in-depth investigation of structural transformations under more highly resolved conditions, while the cluster model presented here yields the correct trends in hydrothermal stability. Good agreement was observed between predicted relative stabilities of materials by molecular modeling and experimental results. Fundamental information from these studies has provided insight into how metal composition and coordination, chemical functionality of organic linker, framework dimensionality, and interpenetration affect the relative stabilities of PCP materials. This work suggests that the strength of the bond between the metal oxide cluster and the bridging linker is important in determining the hydrothermal stability of the PCP. Although the flexibility of the framework plays a role, it is not as important as the metal−linker bond strength. This demonstration of alignment between experimental and calculated observations has proven the validity of the method, and the insight derived herein insight facilitates direction in designing ideal MOF materials with improved hydrothermal stability for desired applications.

1. Introduction

Metal organic frameworks (MOFs), also known as porous coordination polymers (PCPs), are high surface area inorganic/organic hybrid materials possessing relatively high thermal stability.[1] As such, PCPs are being evaluated for a number of applications, including gas adsorption and storage,[2] separations,[3] catalysis,[4] and drug delivery.[5] Hydrothermal stability, a combination of thermal stability and resistance to irreversible reaction with water via hydrolysis, is a critical property for commercial sorbents. Damage caused to a sorbent by moisture at process conditions or during regeneration will limit the usefulness of the sorbent. In order to evaluate and predict this important characteristic, herein we describe the development of a laboratory high throughput hydrothermal stability test and a complementary qualitative model to predict the hydrothermal stability for PCPs.

The primary purpose for developing the model was to allow for the prediction of the relative hydrothermal stability of PCPs, rather than a prediction for absolute conditions at which a given PCP would structurally decompose. The model becomes more quantitative when combined with experimental data. In this way, theory can be used to guide experimentalists toward new

(1) (a) Ferey, G. *Chem. Soc. Rev.* **2008**, *37*, 191–214. Ferey, G. *Stud. Surf. Sci. Catal.* **2007**, *168*, 327–374 (Introduction to Zeolite Molecular Science and Practice). (b) Maji, T. K.; Kitagawa, S. *Pure Appl. Chem.* **2007**, *79*, 2155–2177. (c) Rowsell, J. L. C.; Yaghi, O. M. *Microporous Mesoporous Mater.* **2004**, *73*, 3–14.

(2) (a) Zhao, D.; Yuan, D.; Zhou, H.-C. *Energy Environ. Sci.* **2008**, *1*, 222–235. (b) Wong-Foy, A. G.; Matzger, A. J.; Yaghi, O. M. *J. Am. Chem. Soc.* **1998**, *120*, 3494–3495. (c) Li, H.; Eddaouddi, M.; Groy, T. L.; Yaghi, O. M. *J. Am. Chem. Soc.* **1998**, *120*, 8571–8572.

(3) (a) Alaerts, L.; Maes, M.; Jacobs, P. A.; Denayer, J. F. M.; De Vos, D. E. *Phys. Chem. Chem. Phys.* **2008**, *10*, 2979–2985. (b) Chen, B.; Liang, C.; Yang, J.; Contreras, D. S.; Clancy, Y. L.; Lobkovsky, E. B.; Yaghi, O. M. *Angew. Chem., Int Ed.* **2006**, *45*, 1390–1393. (c) Bae, Y. S.; Mulfort, K. L.; Frost, H.; Ryan, P.; Punnathanam, S.; Broadbelt, L. J.; Hupp, J. T.; Snurr, R. Q. *Langmuir* **2008**, *24*, 8592–8598. (d) Bae, Y. S.; Farha, O. K.; Spokoyny, A. M.; Mirkin, C. A.; Hupp, J. T.; Snurr, R. Q. *Chem. Commun.* **2008**, 4135–4137. (e) Li, J.-R.; Kuppler, R. J.; Zhou, H.-C. *Chem. Soc. Rev.* **2009**, *38*, 1477–1504. (f) Bae, Y. S.; Farha, O. K.; Hupp, J. T.; Snurr, R. Q. *J. Mater. Chem.* **2009**, *19*, 2131–2134.

(4) (a) Maksimchuk, N. V.; Timofeeva, M. N.; Melgunov, M. S.; Shmakova, A. N.; Yu., A.; Chesalova, D. N.; Dybtsev, V. P.; Fedin, O. A.; Kholdeeva, *J. Catal.* **2008**, *257*, 315–323. (b) Horike, S.; Dinca, M.; Tamaki, K.; Long, J. R. *J. Am. Chem. Soc.* **2008**, *130*, 5854–5855. (c) Shultz, A. M.; Farha, O. K.; Hupp, J. T.; Nguyen, S. T. *J. Am. Chem. Soc.* **2009**, *131*, 4204–4205. (d) Lee, J.-Y; Farha, O. K.; Roberts, J; Scheidt, K. A.; Nguyen, S.; Hupp, J. T. *Chem. Soc. Rev.* **2009**, *38*, 1450–1459.

(5) Horcajada, P.; Serre, C.; Maurin, G.; Ramsahye, N. A.; Balas, F.; Vallet-Regí, M.; Sebban, M.; Taulelle, F.; Férey, G. *J. Am. Chem. Soc.* **2008**, *130*, 6774–6780.

10.1021/ja9061344 CCC: $40.75

structures as well as away from PCPs that are predicted to be unstable with respect to hydrolysis.

The reaction of water with the metal oxide clusters (hydration) in metal organic frameworks could involve ligand displacement and/or hydrolysis. The ligand displacement reaction involves inserting a water molecule into a metal−ligand bond of the PCP as shown in eq 1:

$$M - L + H_2O \rightarrow M - (OH_2)\cdots L \quad (1)$$

During the hydrolysis reaction, the metal−ligand bond is broken and water dissociates into a hydroxide anion and proton. The hydroxide anion bonds to the metal, and the proton binds to the displaced ligand as shown in eq 2:

$$M - L + H_2O \rightarrow M - (OH) + LH \quad (2)$$

Greathouse and Allendorf used empirical force fields and molecular dynamics to simulate the interaction of water with IRMOF-1 to predict that IRMOF-1 is unstable once exposed to minor water exposure.[6] Although these calculations are consistent with the observed hydrothermal instability of IRMOF-1 (vide infra), the force fields used in these simulations are not realistic models of breaking and forming bonds during reaction.

Quantum mechanics was used to model the reaction of water with metal organic frameworks to avoid force field issues. Quantum mechanics does not require parameters for every metal−ligand pair and can model hydrolysis reactions which involve the breaking of O−H bonds. Unfortunately, quantum mechanics requires orders of magnitude more computational effort than force field calculations. However, PCPs are amenable to simplified cluster studies since much of the organic linker is not directly involved in the reaction between water and metal oxide clusters. A simple model of PCP connectivity can be built by replacing a linking ligand with a much simpler linker containing the same functional group bound to the metal. For example, one can replace terephthalate with acetate in MOF-5 (aka IRMOF-1) to yield the $Zn_4O(O_2CCH_3)_6$ cluster. Thus, the $Zn_4O(O_2CH_3)_6$ cluster should have similar chemistry to the $Zn_4O(O_2CR)_6$ clusters in the IRMOF-1 series. An added benefit is that PCP frameworks are flexible,[7] which suggests that the framework may not impose significant constraints on the metal oxide cluster during reactions. This framework flexibility also implies that a cluster approach to modeling the chemistry of PCPs may be valid.

2. Experimental Section

2.1. General Synthetic Procedures. All reagents and solvents employed were commercially available as follows and used as supplied without further purification from the following sources: Sigma-Aldrich, *N,N′*-dimethylformamide ≥99.8% (DMF), zinc nitrate hexahydrate 98% ($Zn(NO_3)_2\cdot 6H_2O$), copper nitrate hemipentahydrate 98% ($Cu(NO_3)_2\cdot 2.5H_2O$), chromium(III) nitrate nonahydrate 99% ($Cr(NO_3)_3\cdot 9H_2O$), benzenedicarboxylic acid 98% (H_2BDC), 2,5-dihydroxyterephthalic acid 98% (H_2DOBDC), 1,3,5-benzenetricarboxylic acid 95% (H_3BTC), trimethyl 1,3,5-benzenetricarboxylate 98% (Me_3BTC), 4,4′-dipyridyl 98% (bipy), 1, 4-diazabicyclo[2.2.2]-octane 98% (DABCO), 2-methylimidazole 99% (H-MeIM), methanol (MeOH); Acros, triethylamine 99% (TEA); Aaper, ethyl alcohol 200 proof (EtOH).

IRMOF-1, $Zn_4O(BDC)_3$, was synthesized according to the literature procedure.[8] The crystals were collected by repeated centrifugation and thorough DMF washing (3×, 1 h each) followed by dry acetone washing (4−5 times, 4−5 days each). The white powder was then dried at 100 °C in a furnace with flowing nitrogen for at least 4 h. All samples were stored in a desiccator to avoid moisture adsorption. Before gas adsorption analysis, IRMOF-1 was heated to 125 °C under dynamic vacuum for 16 h.

MOF-69C, $Zn_3(OH_2)(BDC)_2$, was synthesized according to the literature procedure.[9] The crystals were exchanged with DEF (2×) and $CHCl_3$ (5×, 4 days), solvent was decanted, and the resultant material was dried at 100 °C in a furnace with flowing nitrogen for at least 4 h. All samples were stored in a desiccator to avoid moisture adsorption.

Zn-MOF-74, Zn_2(DOBDC), was synthesized according to the literature procedure.[9] The crystals were exchanged with DMF (2×) and MeOH (5×, 6 days), solvent was decanted, and the resultant material was dried at 100 °C in a furnace with flowing nitrogen for at least 4 h. All samples were stored in a desiccator to avoid moisture adsorption. Before gas adsorption analysis, Zn-MOF-74 was heated to 150 °C under dynamic vacuum for 16 h.

MOF-508b, $Zn(BDC)(bipy)_{0.5}$, was synthesized according to literature procedures.[10] The crystals were exchanged with DMF (2×) and hexanes (2×, 2 days), filtered, and washed with hexanes before being dried at 100 °C in a furnace with flowing nitrogen for at least 4 h. All samples were stored in a desiccator to avoid moisture adsorption. Before gas adsorption analysis, MOF-508b was heated to 200 °C under dynamic vacuum for 16 h.

Zn-BDC-DABCO, $Zn_2(BDC)_2$(DABCO), was synthesized according to literature procedures.[11] The white powder was collected by filtration, washed with DMF, and resuspended in MeOH. The solvent was exchanged with stirring (11×, 5 days), and the material was dried at 100 °C in a furnace with flowing nitrogen for at least 4 h. All samples were stored in a desiccator to avoid moisture adsorption. Before gas adsorption analysis, Zn-BDC-DABCO was heated to 125 °C under dynamic vacuum for 25 h.

HKUST-1, $Cu_3(BTC)_2(H_2O)_3$,[12a] was synthesized solvothermally using EtOH as the solvent according to the literature procedure.[12b] The blue powder was filtered and washed with EtOH before being dried at 100 °C in a furnace with flowing nitrogen for at least 4 h, resulting in a purple powder. All samples were stored in a desiccator to avoid moisture adsorption. Before gas adsorption analysis, HKUST-1 was heated to 170 °C under dynamic vacuum for 16 h.

Cr-MIL-101, $Cr_3F(H_2O)_2O(BDC)_3\cdot nH_2O$, was synthesized and ethanol activated and dried according to the literature procedure.[13] Before gas adsorption analysis, Cr-MIL-101 was heated to 100 °C under dynamic vacuum for 16 h.

Al-MIL-110, $Al_8(OH)_{12}\{(OH)_3(H_2O)_3\}[BTC]_3$, was synthesized, filtered, water washed, and dried according to literature procedures.[14] Before gas adsorption analysis, Al-MIL-110 was MeOH activated according to literature procedures and heated to 85 °C under dynamic vacuum overnight.

(6) Greathouse, J. A.; Allendorf, M. D. *J. Am. Chem. Soc.* **2006**, *128*, 10678–10679.
(7) (a) Uemura, K.; Matsuda, R.; Kitagawa, S. *J. Solid State Chem.* **2005**, *178*, 2420–2429. (b) Fletcher, A. J.; Thomas, K. M.; Rosseinsky, M. J. *J. Solid State Chem.* **2005**, *178*, 2491–2510. (c) Ferey, G.; Serre, C. *Chem. Soc. Rev.* **2009**, *38*, 1380–1399.
(8) Li, H.; Eddaoudi, M.; O'Keeffe, M.; Yaghi, O. M. *Nature* **1999**, *402*, 276–279.
(9) Rosi, N. L.; Kim, J.; Eddaoudi, M.; Chen, B.; O'Keeffe, M.; Yaghi, O. M. *J. Am. Chem. Soc.* **2005**, *127*, 1504–1518.
(10) (a) Chen, B.; Liang, C.; Yang, J.; Contreras, D. S.; Clancy, Y. L.; Lobkovsky, E. B.; Yaghi, O. M.; Dai, S. *Angew. Chem., Int. Ed.* **2006**, *45*, 1390–1393. (b) Chun, H.; Dybstev, D. N.; Kim, H.; Kim, K. *Chem.—Eur. J.* **2005**, *11*, 3521–3529. (c) Ma, B.; Mulfort, K. L.; Hupp, J. T. *Inorg. Chem.* **2005**, *44*, 4912–4914.
(11) Dybtsev, D. N.; Chun, H.; Kim, K. *Angew. Chem., Int. Ed.* **2004**, *43*, 5033–5036.
(12) (a) Chui, S.-Y.; Lo, M.-F.; Charmant, J. P. H.; Orpen, A. G.; Williams, I. D. *Science* **1999**, *283*, 1148–1150. (b) Hartmann, M.; Kunz, S.; Himsl, D.; Tangermann, O. *Langmuir* **2008**, *24*, 8634–8642.
(13) Ferey, G.; Mellot-Draznieks, C.; Serre, C.; Millange, F.; Dutour, J.; Surble, S.; Margiolaki, I. *Science* **2005**, *309*, 2040–2042.

Al-MIL-53, Al(OH)[BDC], was synthesized, filtered, water washed, and dried according to literature procedures.[15] Calcination was performed at 375 °C for 6 h under nitrogen to remove occluded BDC species from pores. Before gas adsorption analysis, Al-MIL-110 was heated to 150 °C under dynamic vacuum overnight.

$Zn(MeIM)_2 \cdot (DMF) \cdot (H_2O)_3$, (named ZIF-8 in ref 16b) was synthesized, purified by density separation, methanol activated, and dried according to the literature procedure.[16] Before gas adsorption analysis, ZIF-8 was heated to 300 °C under dynamic vacuum for 18 h.

2.2. High Throughput Hydrothermal Stability Testing. For hydrothermal stability testing, the solvent-exchanged, dried PCP material is used as received (if in powder form) or placed through a mesh screen if larger agglomerates are present. A small quantity ($<^1/_2$ cm height) is loaded into each of the quartz tubes, and the material is heated to a specified temperature overnight in flowing nitrogen. The high throughput heat treatment unit contains 48 parallel heaters arrayed in six rows and eight columns. Steam is generated by combining a liquid source and a gas source inside heated quartz blenders. The steam is then delivered by row to the 48 fritted quartz tube reactors.

For PCP materials, the steaming experiments were designed to split one batch of material among several reactors under different conditions. Replicate conditions were included in the experimental design when material quantities allowed. The conditions were chosen to cover as wide a range as possible of temperatures and steam levels tailored to each material, in order to determine hydrothermal stability limits evaluated by crystallinity and phase changes through X-ray diffraction (XRD).

PCP samples were taken out of a dry environment and handled in air while loading into the unit, keeping the loading time as short as possible to minimize adsorption of water from the air. Once loaded, the samples were kept under flowing nitrogen throughout the run. Each steaming run typically had an overnight "activation" hold under nitrogen flow at a temperature particular to each material, followed by a ramp to the target steam temperature. Steam (nitrogen and water mix) was introduced for 2 h and then cut off, at temperature, to purge the atmosphere for 30 min. Samples were then cooled to room temperature, quickly unloaded from the unit in air, photographed, and submitted for GADDS powder XRD analysis. Data were collected on a Bruker AXS GADDS diffractometer, which is equipped with an automated XYZ stage for sample positioning. Data were collected over the 2Θ range from at least 4° to 35°, in 0.05° steps via 30 s scans.

2.3. Other Characterization Details. For bulk PCP samples, and for those samples not analyzed via the high-throughput diffractometer described above, powder X-ray diffraction (XRD) patterns were obtained on a Scintag XDS 2000 (Cu Kα) over the range 2−56° 2θ with a step size of 0.02° 2θ and a 1 s integration time per step. Elemental analysis was accomplished by ICP and Leco (C, N). Sample surface area and pore volume measurements were determined from N_2 40-point isotherm data using a Micromeritics ASAP 2400 instrument. Samples were activated before analysis as described in the Introduction. Micropore volumes were calculated using the *t*-plot method. Microscopic characterization was carried out on JEOL 7401 (high resolution), Zeiss EVO 50, and/or Hitachi S-2600N scanning electron microscopes.

Table 1. Hydrolysis (hyd), Ligand Displacement (disp) Reaction and Activation Energy of Displacement (in kcal/mol) Predicted for Reactions of Water with PCP Cluster Models

complex	PCP	ΔE_{hyd}	ΔE_{disp}	$\Delta E^{\ddagger}_{disp}$
Zn_4OAc_6	MOF-5	−7.3	0.1	11.6
$Cu_2Ac_4(H2O)_2$	HKUST-1	−8.8	13.9	28.9
$Cr_3OAc_6F(H_2O)_2$	MIL-101	−26.9	7.9	35.8
$Zn_{12}(mIM)_{16}Cl_8$	ZIF-8	−4.0	−3.2	55.7

2.4. Calculational Details. The quantum mechanical calculations were carried with the program DMOL3 from Accelrys, Inc.[17] The DND basis set with medium precision was used. The gga(p91) functional was used.[18] Transition states were determined with QST/LST reaction path methods.[19] Models involving second or third row transition metals and lanthanides included scalar relativistic effects.[20]

3. Results

3.1. Test of Cluster Model. The cluster approach was tested by predicting energies of ligand displacement and hydrolysis and activation energies for ligand displacement for cluster models of four different PCPs with quantum mechanical calculations and by comparing the energies with experimentally observed hydrothermal stability. The metal−oxide acetate clusters $Zn_4O(O_2CCH_3)_6$, $Cu_2(O_2CCH_3)_4$, and $Cr_3O(CO_2CH_3)_6F$ and imidizolate cluster $Zn_{12}(mIM)_{16}Cl_8$ were used as models of the metal oxide clusters in MOF-5,[8] HKUST-1,[12] and MIL-101,[13] and ZIF-8,[16] respectively. Two water molecules were added to the cluster models of $Cu_2(O_2CCH_3)_4$ and $Cr_3O(CO_2CH_3)_6F$ to complete the geometric coordination of the metal atoms before hydrolysis or ligand displacement reactions. The predicted energies for hydrolysis and ligand displacement are shown in Table 1. The activation energy for ligand displacement is included in Table 1, as well. Note that the predicted energies for hydrolysis and ligand displacement are uncorrelated and predicted activation energies for ligand displacement correlate with the observed hydrothermal stabilities for MOF-5, HKUST-1, and MIL-101. This implies that hydrothermal stability in under kinetic control in our experiments.

Geometries of predicted reactants, products, and transition states for ligand displacement reaction in the three carboxylate cluster complexes are shown in Figure 1 and are included in the Supporting Information. Note that water molecules in the reactant complexes tend to have their protons directed at the oxygen of the cluster complex which form hydrogen bonds with the complex. Hydrogen bonding appears to be an important part of the interaction between water in the second coordination shell and the metal oxide cluster. The carboxylate in the transition state of all these complexes has changed from η^2 to η^1 coordination and has opened up a coordination site on the metal for the water molecule. The water molecule ends up bridging the metal and the carboxylate with a proton pointing at the displaced oxygen atom of the carboxylate and the oxygen coordinated to the metal.

3.2. Experimental Hydrothermal Stability Testing. The most critical test of the cluster model is validation via comparison to

(14) (a) Volkringer, C.; Popov, D.; Loiseau, T.; Guillou, N.; Ferey, G.; Haouas, M.; Taulelle, F.; Mellot-Draznieks, C.; Burghammer, M.; Riekel, C. *Nat. Mater.* **2007**, *6*, 760–764. (b) Haouas, M.; Volkringer, C.; Loiseau, T.; Ferey, G.; Taulelle, F. *Chem.—Eur. J.* **2009**, *15*, 3139–3146.

(15) Loiseau, T.; Serre, C.; Huguenard, C.; Fink, G.; Taulelle, F.; Henry, M.; Bataille, T.; Ferey, G. *Chem.—Eur. J.* **2004**, *10*, 1373–1382.

(16) (a) Huang, X.-C.; Lin, Y.-Y.; Zhang, J.-P.; Chen, X.-M. *Angew. Chem., Int Ed.* **2006**, *45*, 1557–1559. (b) Park, K. S.; Ni, Z.; Cote, A. P.; Choi, J. Y.; Huang, R.; Uribe-Romo, F. J.; Chae, H. K.; O'Keeffe, M.; Yaghi, O. M. *Proc. Natl. Acad. Sci. U.S.A.* **2006**, *103*, 10186–10191.

(17) (a) Delley, B. *J. Chem. Phys.* **1990**, *92*, 508–517. (b) Delley, B. *J. Chem. Phys.* **2000**, *113*, 77567764. DMol^3 is available as part of Materials Studio from Accelrys Inc. Version 4.2.1. The DN basis set and medium precision were used in these calculations.

(18) Perdew, J. P.; Wang, Y. *Phys. Rev. B* **1992**, *45*, 13244–13249.

(19) Henkelman, G.; Jonsson, H. *J. Chem. Phys.* **2000**, *113*, 9978–9985.

(20) (a) Koelling, D. D.; Harmon, B. N. *J. Phys. C: Solid State Phys.* **1977**, *10*, 3107–3114. (b) Douglas, M.; Kroll, N. M. *Ann. Phys. (San Diego)* **1974**, *82*, 89–155.

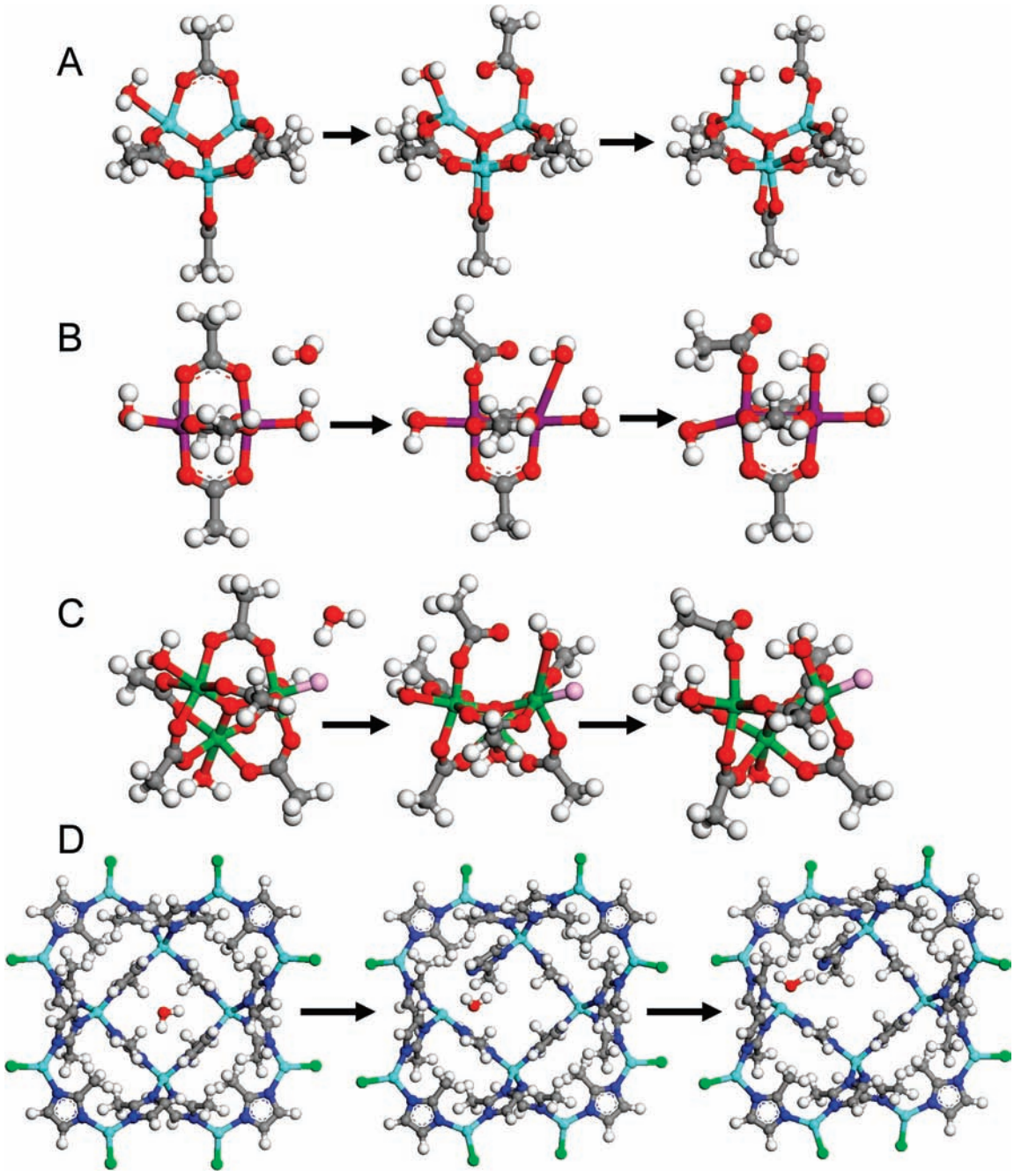

Figure 1. Ligand displacement reaction for MOF-5 (A), HKUST-1 (B), MIL-101 (C), and ZIF-8 (D). Structures represent reactant, transition state, and hydrolysis product clusters for each PCP, respectively. Color scheme: gray, C; red, O; white, H; light blue, Zn; purple, Cu; dark green, Cr; pink, F; light green, Cl; and dark blue, N.

experimentally derived results. Experimental hydrothermal stability data were generated by subjecting PCP samples to relevant steaming conditions in a combinatorial chemistry heat treatment unit followed by analysis in a high-throughput X-ray diffractometer. Initial experimental work showed that MOF-5 is unstable with respect to even low levels of water, particularly at low temperature. This observation is consistent with other literature reports.[21] For example, XRD patterns for MOF-5 exposed to flowing dry nitrogen for 2 h at temperatures from 40 to 100 °C show no structural degradation (Figure 2A). However, exposure of MOF-5 to the same conditions but with 1 mol % steam rather than dry nitrogen resulted in structural transformation, as evidenced by XRD (Figure 2B).[22] XRD also suggests that pure BDC linker did not recrystallize within the pore structure of MOF-5 as a result of the steaming process. This indicates that the hydration reaction does not necessarily break down the framework completely. Surface area loss was also significant (see Supporting Information, Table S1).

HKUST-1 was significantly more stable to steam than MOF-5. No structural transformation was observed by XRD at 50 mol % steam at temperatures up to 200 °C (Figure 3, left panels).

(21) Huang, L.; Wang, H.; Chen, J.; Wang, Z.; Sun, J.; Zhao, D.; Yan, Y. *Microporous Mesoporous Mater.* **2003**, *58*, 105–114.

(22) (a) Hausdorf, S.; Wagler, J.; Mossig, R.; Mertens, F. O. R. L. *J. Phys. Chem. A* **2008**, *112*, 7567–7576. (b) Kaye, S. S.; Dailly, A.; Yaghi, O. M.; Long, J. R. *J. Am. Chem. Soc.* **2007**, *129*, 14176–14177.

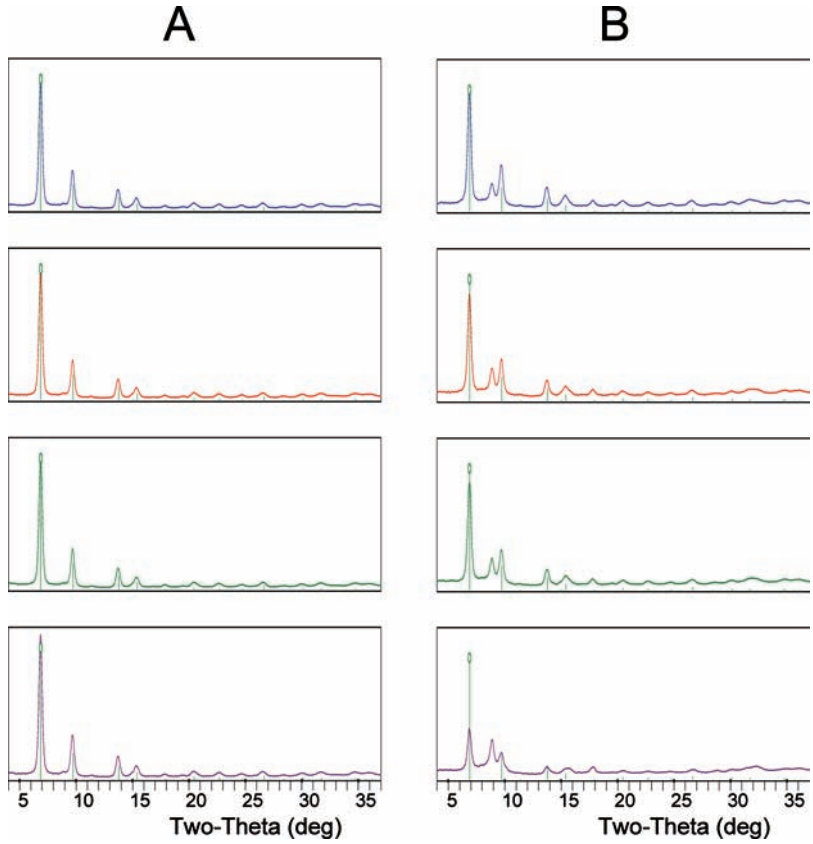

Figure 2. XRD patterns for MOF-5 under dry nitrogen (A) and 1 mol % steam at 40, 60, 80, and 100 °C (bottom to top).

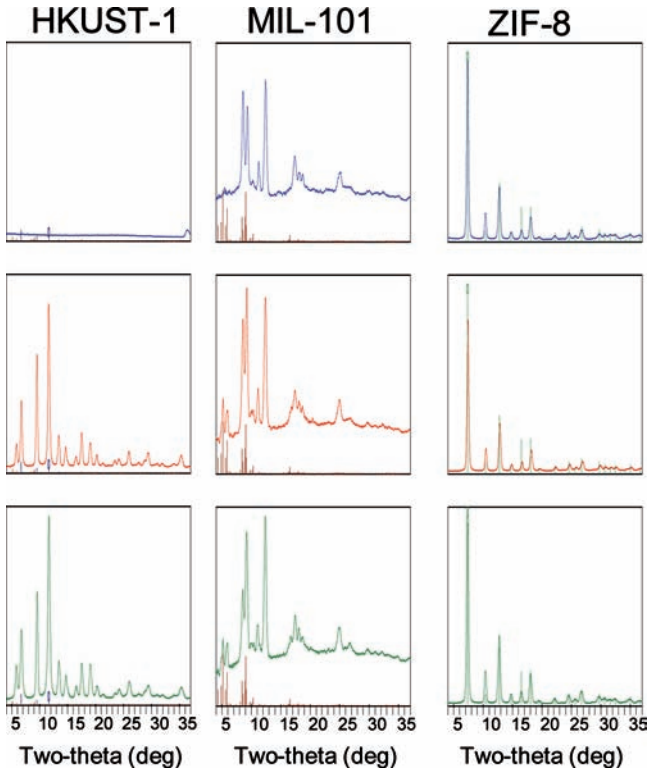

Figure 3. XRD patterns for HKUST-1, MIL-101 (linker impurity at 10.8° 2θ), and ZIF-8 under 50 mol % steam for 2 h at 85, 200, and 300 °C (bottom to top). Small sticks in each spectrum represent simulated reflections generated from literature CIF files for HKUST-1,[12a] MIL-101,[13] and ZIF-8.[16b]

Since HKUST-1 thermally decomposes irreversibly above about 250 °C,[9] the spectrum for the 300 °C treatment shows complete loss of structure (Figure 3, top left). In the case of MOF-5, surface area (Table S1) loss is evident, even after mild temperature exposure to 25 mol % steam. SEM images also show evidence of structural transformation (see Supporting Information, section V).

MIL-101 begins to show transformation to a higher temperature structure between ~250 and 300 °C, as evidenced by the steady loss of low angle reflections in XRD spectra (see Figure 3, center panels). MIL-101 also changes from its characteristic green color to brown as the temperature of the steaming experiment is increased (see Figure S1). It is interesting that color changes are only observed (from green to brown) as temperature increases across all steam levels. Color changes are not observed for increasing steam levels at each temperature level. Again, overall physical properties of steamed MIL-101 are affected by the relative exposure to steam (Table S1 and SEM images in Supporting Information).

A PCP constructed from imidizolate rather than carboxylate linkers, $Zn(MeIM)_2 \cdot (DMF) \cdot (H_2O)_3$ (also known as ZIF-8), was also prepared and exposed to hydrothermal treatment.[16] Unlike MOF-5, HKUST-1, and MIL-101, this PCP was not significantly degraded structurally at 50 mol % steam at up to 300 °C (Figure 3, right panels). This result is in line with the literature[16b] and the $\Delta E^{\ddagger}$ (55.7 kcal/mol) predicted by modeling. While SEM images show a slight change in morphology, the surface area of ZIF-8 remains unchanged after steaming (see Supporting Information, Table S1 and section V).

4. Discussion

4.1. Hydrothermal Stability. Regarding hydrothermal stability, it is clear from results reported above that ZIF-8 is unique when compared to the other PCPs discussed above. That is, ZIF-8 was observed and calculated to be more hydrothermally stable than PCPs bridged by carboxylates. In the case of carboxylates, the ligand has changed from η^2 to η^1 bonding during the ligand displacement reaction. In other words, the formally three-center, two-electron bond between the metal and two oxygen atoms of the linker has become a two-center, two-electron bond between the metal and only one oxygen atom of the linker. The carboxylate anion can accommodate this changing from two bonds formed between the metal and two oxygen atoms with $-^1/_2$ charge and one bond formed between the metal and an oxygen with a -1 charge. This change in the metal carboxylate bonding lowers the activation and reaction energy during the ligand displacement reaction. In the case of imidizolates, the ligands are bonded η^1 to the metal and must break one of two metal−ligand bonds during the ligand displacement reaction. Imidazolates will tend to be more hydrothermally stable than carboxylates because a metal−ligand bond must be broken, while carboxylates can still maintain a metal−ligand bond during ligand displacement reaction. PCPs synthesized from linkers which are bonded η^1 to the metal will be more stable than linkers which are bonded η^2 to the metal.

It was also observed that PCPs containing 6-coordinate (usually octahedral) metal ions tend to be more stable than those containing 4-coordinate (usually tetrahedral) metal ions. One explanation is that more space is available for a water molecule to coordinate to a tetrahedrally coordinated metal than a metal with octahedral coordination. This in turn lowers the barrier for linker displacement. For example, MOF-5 is less stable than Zn-MOF-74.[9] This trend should hold for other bridging linkers as well. For instance, the PCPs composed of infinite rods of metal oxides were modeled as 1D infinite chains.[9] These points will be discussed in more detail below.

It is also important to consider the effect of the oxidation state of the metal (ZIF-8) or metal cluster (MOF-5, HKUST-1, MIL-101) during hydration. It is expected that the higher the oxidation state on the metal or metal cluster, the higher the relative stability is (or will be) toward reaction with water. In order to compare clusters to individual metals, one can take the charge of the cluster and divide it by the total number of metals in the cluster. For example, for the Zn_4O^{6+} cluster found in MOF-5, the relative positive charge per Zn is 1.5, while the relative positive charges per Cu in HKUST-1 and Cr in MIL-101 are 2.0 in each case. Qualitatively, this suggests that the secondary building units (SBUs) of HKUST-1 and MIL-101 should form more stable bonds with their respective linkers than the MOF-5 SBU does with BDC linkers. In a similar way, one can reason that individual Zn atoms which possess a 2+ oxidation state in ZIF-8 will form stronger metal−linker bonds than those between the Zn_4O^{6+} SBU and six BDC linkers. This would lead us to predict that ZIF-8 would be more stable to hydration reactions than MOF-5. However, it should be noted that this prediction does not take into account the obvious difference between imidizolate nitrogen atom−metal bonds and carboxylate oxygen−metal bonds strength. As mentioned above, the zinc−nitrogen bonds in ZIF-8 would be expected to be stronger than the zinc−oxygen bonds in MOF-5.

For the three metal carboxylate PCPs, another simple way to predict PCP stability to water would be to consider relative metal−oxygen strengths from common metal oxides. The trend for divalent first-row transition metal−oxygen bond strengths in metal oxides is to decrease as one proceeds from, e.g., FeO (468 kJ/mol) to CrO (374 kJ/mol) to CuO (372 kJ/mol) to ZnO (365 kJ/mol). See Table S2. From these values alone we might predict HKUST-1 would be slightly more stable with respect to reaction with water than MOF-5, and because MIL-101 has trivalent Cr (Cr_2O_3 at 465 kJ/mol), we might predict it to be somewhat more moisture-stable than HKUST-1. These predictions are qualitatively correct, but the subtleties of the overall oxidation state and resultant stability of the SBUs rather than the metal cations are not revealed in this simple analysis. It is only upon combining these concepts that one would predict that MOF-5 is significantly less stable than HKUST-1, and that MIL-101 is likely more stable than HKUST-1 (although not to the degree expected on the basis of metal−oxygen bond strengths alone).

Note that ligand substitution rates (kinetics) have not been considered here. Our model takes into account only the equilibrium ground and transition state configurations. This means that even though it would be expected that Cr^{3+}, being inert[23] with respect to ligand exchange reactions in general, might react so slowly with water that complexes containing this cation would be expected to be more stable with respect to reaction with water vapor than other more labile trivalent cations such as Fe^{3+} and Al^{3+}. Experimentally, "accelerated" screening at elevated temperature and long exposure times ensure operation under thermodynamic rather than kinetic control. Regarding the group of M^{2+} cations discussed here, ligand exchange reaction rates should be rapid and similar enough among the group to neglect kinetic considerations for hydrolysis and ligand displacement.[24]

4.2. Virtual High Throughput Screening of PCPs. In the first section, it was established that the cluster model can effectively rank the relative stability of a PCP with respect to reaction with water among four reference PCPs. To further develop the model, a scan of activation energies for ligand displacement for several other PCPs was then carried out. A sampling of those, for which experimental results were also determined, will be discussed here (Table 2). The samples, which include MOF-5, HKUST-1, and MIL-101 as reference points, are listed from the least (MOF-69C[9]) to most (Al-MIL-53[15]) stable with respect to reaction with water vapor, as determined via VHTS. The relative ranking determined experimentally is slightly different. Comments regarding the experimental results appear in the last column in Table 2.

4.3. SBU Contributions to Hydrothermal Stability. In attempting to explain the results of the modeling and experimental data, several important factors to consider include dimensionality of the metal-containing SBU, stability of the SBU itself, and SBU connectivity in the PCP structure. All of these factors, and perhaps several others, determine the resultant effect on stability with respect to reaction with water vapor. While the Zn_4O^{6+} cluster SBU itself (Figure 4a) is stable in solution,[25] the SBU bonds with BDC in a 0D (i.e., all metal SBUs are connected to linkers only and not to other metal-containing

(23) See general comparisons provided in the following: (a) Douglas, B. E.; McDaniel, D. H.; Alexander, J. J. *Concepts and Models of Inorganic Chemistry*; John Wiley and Sons: New York, 1983; pp 334−335. (b) Baes, C. F., Jr.; Mesmer, R. E. *Hydrolysis of Cations*; Krieger Publishing: Malabar, FL, 1976; pp 407−409.
(24) Gray, H. B.; Langford, C. H. *Chem. Eng. News* **1968**, 68.
(25) Clegg, W.; Harbron, D. R.; Homan, C. D.; Hunt, P. A.; Little, I. R.; Straughan, B. P. *Inorg. Chim. Acta* **1991**, *186*, 51–60.

Table 2. Characteristics, Calculated Energy of Activation for Ligand Displacement by Water Vapor, and Experimentally Determined Maximal Structural Integrity for PCPs Modeled and/or Evaluated Experimentally in This Study

PCP	linker	SBU[a]	SBU detail	inorg connect[b]	$\Delta E^{\ddagger}_{disp}$ from VTHS[c] (kcal/mol)	experimental summary[d]
MOF-69C	BDC[e]	chain	two 4- and one 6-coordinate Zn	1D	unstable[k]	0% steam, ambient
MOF-5	*BDC*	Zn_4O^{6+}	Zn tetramer	*0D*	11.6	2% steam, 40 °C
MOF-508B	BDC and bipy[f]	Zn_2^{2+}	Zn paddlewheel	0D	18.9	5% steam, 100 °C
MIL-110	Me_3BTC[g]	$Al_8(OH)_{15}^{9+}$	Al-octamer	0D	21.2	50% steam, 300 °C
HKUST-1	*BTC*[h]	Cu_2^{2+}	Cu paddlewheel	*0D*	28.9	50% steam, 200 °C
Cr-MIL-53	BDC	chain	corner-shared octahedral	1D	30.5	n.a.
MIL-101	BDC	Cr_3OF^{6+}	Cr trimer	0D	35.8	50% steam, 325 °C
MOF-74	dhBDC[i]	chain	edge-shared octahedral	1D	42.0	50% steam, 325 °C
Al-MIL-53	BDC	chain	corner-shared octahedral	1D	43.4	25% steam, 350 °C or 50% steam, 225 °C
ZIF-8	MeIm[j]	Zn^{2+}	tetrahedral zinc ions	0D	58.5	50% steam, >350 °C

[a] Metal-containing secondary building unit. [b] Number of dimensions into which inorganic-only connections are made. [c] Virtual high throughput screening. [d] Most severe conditions at which structural loss is not observed. [e] Benzenedicarboxylate. [f] 4,4′-Bipyridine. [g] Trimethyl 1,3,5-benzenetricarboxylate. [h] Benzentricarboxylate. [i] Dihydroxybenzenedicarboxylate. [j] Methylimidizolate. [k] During the hydration reaction simulation, when the MOF-69C cluster was saturated with water, more than one acetate ligand was displaced with no energy barrier. As such, MOF-69C was unstable during the calculation, and therefore was predicted to hydrothermally unstable in the laboratory.

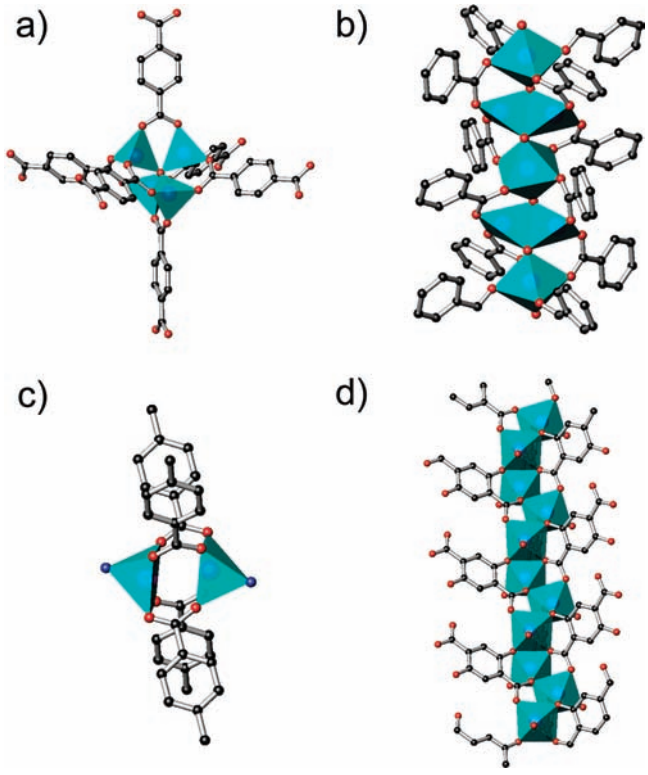

Figure 4. Secondary Building Units (SBUs) for Zn^{2+}-containing PCPs: (a) Zn4O6+ for MOF-5, (b) alternating pairs of edge-sharing tetrahedral and edge-sharing octohedra in chain formation for MOF-69C, (c) square-pyramidal Zn2 paddlewheels in MOF-508B and Zn-BDC-DABCO, and (d) chains of edge-sharing Zn octahedral in MOF-74.

Scheme 1

$$3[Zn_4O(BDC)_3] + 5H_2O \longrightarrow 4[Zn_3(OH)_2(BDC)_2] + H_2BDC$$

MOF-5 **MOF-69C**

SBUs) fashion are somewhat unstable with respect to reaction with water vapor. Other Zn^{2+}-containing SBUs have been found to be even more unstable with respect to reaction with water. For example, MOF-69C, which can be prepared directly from MOF-5 by adding water to a DEF solution and allowing crystals to transform over 1 week (Scheme 1), cannot be exposed to any moisture or heat treatment at all without complete crystal degradation. In this case we suspect that in addition to ligand displacement as described above, the SBU itself is susceptible

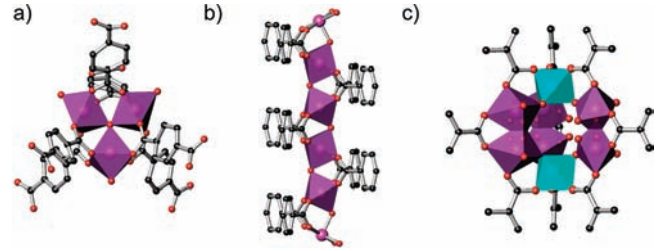

Figure 5. SBUs for M^{3+} (M = Al or Cr) containing PCPs: (a) Cr_3-μ-OF^{6+} trimers in MIL-101, (b) chains of corner-sharing octahedral in Cr- or Al-MIL-53, and (c) $Al_8(OH)_{15}^{9+}$ octamers in MIL-110.

to thermal degradation as well as reaction with water. This may be due to the alternating pairs of edge-sharing, 4-coordinate zinc cations and a 6-coordinate, corner-only-sharing zinc cation connected in one-dimensional chains present in the MOF-69C SBU (Figure 4b). The apexes are likely weak points in this SBU. Another recent report describes additional MOF-5-related transformations in the presence of water and other reactants.[18a]

Alternatively, MOF-508b (an interpenetrated structure)[10] or Zn-BDC-DABCO (noninterpenetrated),[11] both of which contain SBUs of two 5-coordinate zinc cations bridged in a paddlewheel-type configuration (Figure 4c, such as in HKUST-1) to form 0D PCP structure types, were calculated to be only slightly more stable with respect to reaction with water than MOF-5. HKUST-1 is predicted and found to be more stable with respect to reaction with water vapor than the Zn^{2+}-containing PCPs, which is consistent with the general observation that Cu^{2+} aqueous coordination complexes are more stable than corresponding Zn^{2+} complexes.[26]

Another Zn-containing SBU is the infinte rod present in MOF-74.[16] In this PCP, the metals exist as edge-sharing octahedra bridged by the carboxylic acid and hydroxyl functional groups on the dihydroxybenzenedicarboxylic acid (dhBDC) linker (Figure 4d). In contrast to the weakly assembled chains in MOF-69A described above, the chains in MOF-74 are expected to be extremely robust owing to only edge-sharing between metals as well as coordination to two types of functional group on each linker. When solvated, all Zn ions in MOF-74 are 6-coordinate, and therefore it is expected that the zinc−oxygen bonds of the linkers will be less susceptible to displacement by incoming

(26) (a) Bunting, J. W.; Thong, K. M. *Can. J. Chem.* **1970**, *48*, 1654–1656. (b) Pletnev, I. V.; Zernov, V. V. *Anal. Chim. Acta* **2002**, *455*, 131–142.

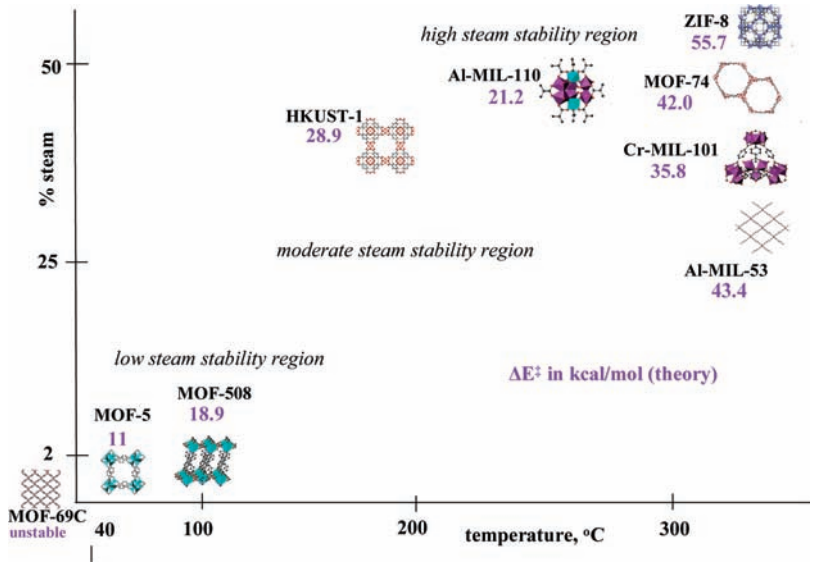

Figure 6. Steam stability map for the four PCPs discussed in this paper. The position of the structure for a given MOF represents its maximum structural stability by XRD measurement, while the energy of activation for ligand displacement by a water molecule determined by molecular modeling is represented by the magenta number (in kcal/mol).

water molecules. In the fully desolvated (activated) state, each Zn also has a coordinatively unsaturated, or open, metal site. When water occupies this site, its removal would involve an endothermic reaction with a relatively large energy barrier to insert it into a metal−ligand bond. Therefore, only water in the second coordination shell is likely to displace a ligand from the metal and damage the framework. Nevertheless, MOF-74 is predicted, and experimentally determined, to possess good stability toward reaction with water. Apparently the open metal site allows the initial water molecules to coordinate without displacing Zn−linker bonds, resulting in the more stable 6-coordinate situation described above. This suggests that a small amount of water exposure may actually increase the overall stability of MOF-74 toward a linker displacement reaction. This observation is consistent with a recent report on exposure of HKUST-1 to water vapor at ambient conditions.[27] In general, we thus observe that for Zn^{2+}-containing SBUs, how the metal is coordinated to other metals within the SBU as well as how each metal is coordinated to the linker(s) present are critical to its stability with respect to reaction with water vapor.

4.4. Metal Valence Contributions to Hydrothermal Stability. In contrast to results discussed so far regarding M^{2+}-containing PCPs, M^{3+}-containing PCPs were calculated to be more resistant than M^{2+}-containing SBUs with respect to reaction with water. The type and configuration of the metal atoms seem to be less significant for M^{3+}-based SBUs. In the first example, the Cr_3-μ-OF^{6+} trimer SBU[28] (Figure 5a) in MIL-101 has already been observed to be fairly stable with respect to the hydration reactions described above. This makes intuitive sense, since the originally reported Cr-containing trimer $Cr_3(CH_3COO)_6OCl(H_2O)_5$[29] is prepared in water, and MIL-101 is prepared hydrothermally in water (solvent) at greater than 200 °C.

The reaction of water vapor with Cr^{3+}-containing Cr-MIL-53 was also modeled.[30] Cr-MIL-53 was found to have comparable stability to reaction with water vapor as Cr-MIL-101 (Table 2). The MIL-53 SBU is composed of infinite chains of corner-sharing M^{3+} octahedra bridged by the BDC linker to form 1D lozenge-shaped pores throughout the PCP (Figure 5b). The Cr−O bonds between the linker and metal atoms in the 1D chains of Cr-MIL-53 are about equally resistant to reaction with water as those of the Cr_3-μ-OF^{6+} trimer in Cr-MIL-101. This suggests that the relative strength of the M−O bond is a more important factor than coordination geometry or valence for M^{3+}-containing-PCPs than for M^{2+}-containing ones. This hypothesis was confirmed by comparing the calculated stability of isostructural Al-MIL-53[15] to Cr-MIL-53. That is, the Al−O bond in alumina is stronger than the Cr−O bond in Cr(III) oxide (514 compared to 447 kJ/mol, see Table S2). It so follows that the calculated values for the activation energy of displacement of BDC linker by water is higher for Al-MIL-53 than for Cr-MIL-53 (43.5 versus 30.4 kcal/mol, see Table 2). Experimentally, the higher stability of Al-MIL-53 toward reaction with water vapor versus Cr-MIL-101 further supports this hypothesis that Al^{3+} PCPs will generally be more hydrothermally stable than Cr^{3+} PCPs.

Such reasoning can be extended to other Al-containing PCPs, such as for MIL-110[14] (Figure 5c). The metal cations in MIL-110 are located in octamer SBUs of Al-octahedra linked through BTC linkers to form 1D channels. There are two trimers of edge-sharing octahedra and two edge-sharing "capping" octahedra per octamer SBU. Formally, the caps are $AlO_3(OH)_3$ and the trimers are $AlO_2(OH)_3(H_2O)$ or $AlO_2(OH)_4$ depending upon termination species present. Experimentally, MIL-110 was determined to have good hydrothermal stability, as Al-MIL-53. See Table 2.

(27) Yazaydýn, A. O.; Benin, A. I.; Faheem, S. A.; Jakubczak, P.; Low, J. J.; Willis, R. R.; Snurr, R. Q. *Chem. Mater.* **2009**, *21*, 1425–1430.
(28) Serre, C.; Millange, F.; Surble, S.; Ferey, G. *Angew. Chem., Int. Ed.* **2004**, *43*, 6286–6289.
(29) Figgis, B. N.; Robertson, G. B. *Nature* **1965**, *205*, 694–695.
(30) (a) Millange, F.; Serre, C.; Ferey, G. *Chem. Commun.* **2002**, 822. (b) Serre, C.; Millange, F.; Thouvenot, C.; Nogues, M.; Marsolier, G.; Louer, D.; Ferey, G. *J. Am. Chem. Soc.* **2002**, *124*, 13519.

5. Conclusions

The modeling and experimental results for the PCPs are compared in a "steam stability map" in Figure 6. The excellent correlation between theory and experiment implies that the activation energies derived from quantum mechanical calculations of cluster models provide a useful estimate of the relative hydrothermal stability of PCPs. Fundamental information from these studies has enabled investigation of how metal composition and coordination, chemical functionality of organic linker, framework dimensionality, and interpenetration affect the relative stabilities of PCP materials. The experimental steaming method allows for high throughput screening of material stability over a broad range of steam levels as well as in-depth investigation of structural transformations under more highly resolved conditions, while the cluster model presented here yields the correct trends in hydrothermal stability. This work suggests that the strength of the bond between the metal oxide cluster and the bridging linker is important in determining the hydrothermal stability of the PCP. Although framework flexibility, which has not been discussed here in detail, may play a role, it is not likely as important as the metal−ligand bond strength. That is, since experimental samples of PCPs are not perfect infinite lattices but powders of small crystallites with significant surface area and defects, the stability of the surface and defects limits the PCP stability. A small cluster model is a better model of defects and the surface than an infinite lattice. This demonstration of alignment between experimental and calculated observations has proven the validity of the method, which should soon be used to select and invent hydrothermally stable PCPs for desired applications.

Acknowledgment. This project was supported by the U.S. Department of Energy through the National Energy Technology Laboratory, under Award DE-FC26-07NT43092.

Supporting Information Available: Images of MIL-101 samples before and after hydrothermal treatment, a summary table of nitrogen adsorption results, a summary of SEM micrographs, and a table of metal−oxygen bond strengths in metal oxides. This material is available free of charge via the Internet at http://pubs.acs.org.

JA9061344